Acta Materialia 113 (2016) 230–244

Contents lists available at ScienceDirect

Acta Materialia

journal homepage: www.elsevier.com/locate/actamat

Full length article

Microstructural stability and mechanical behavior of FeNiMnCr high entropy alloy under ion irradiation

N.A.P. Kiran Kumar [a, *], C. Li [b], K.J. Leonard [a], H. Bei [a], S.J. Zinkle [a, b]

[a] Oak Ridge National Laboratory, Oak Ridge, TN, USA
[b] University of Tennessee, Knoxville, TN, USA

ARTICLE INFO

Article history:
Received 26 February 2016
Received in revised form
29 April 2016
Accepted 3 May 2016
Available online 13 May 2016

Keywords:
High entropy alloy
Radiation-induced segregation
Dislocation loops
Concentrated multi-component solid solution alloy
Irradiation defects

ABSTRACT

In recent years, high entropy alloys (HEAs) have attracted significant attention due to their excellent mechanical properties and good corrosion resistance, making them potential candidates for high temperature fission and fusion structural applications. However there is very little known about their radiation resistance, particularly at elevated temperatures relevant for energy applications. In the present study, a single phase (face centered cubic) concentrated solid solution alloy of composition 27%Fe-28%Ni-27%Mn-18%Cr was irradiated with 3 or 5.8 MeV Ni ions at temperatures ranging from room temperature to 700 °C and midrange doses from 0.03 to 10 displacements per atom (dpa). Transmission electron microscopy (TEM), scanning transmission electron microscopy with energy dispersive x-ray spectrometry (STEM/EDS) and X-ray diffraction (XRD) were used to characterize the radiation defects and microstructural changes. Irradiation at higher temperatures showed evidence of relatively sluggish solute diffusion with limited solute depletion or enrichment at grain boundaries. The main microstructural feature at all temperatures was high-density small dislocation loops. Voids were not observed at any irradiation condition. Nano-indentation tests on specimens irradiated at room temperature showed a rapid increase in hardness ~35% and ~80% higher than the unirradiated value at 0.03 and 0.3 dpa midrange doses, respectively. The irradiation-induced hardening was less pronounced for 500 °C irradiations (<20% increase after 3 dpa). Overall, the examined HEA material exhibits superior radiation resistance compared to conventional single phase Fe-Cr-Ni austenitic alloys such as stainless steels. The present study provides insight on the fundamental irradiation behavior of a single phase HEA material over a broad range of irradiation temperatures.

1. Introduction

High entropy alloys (HEAs) are composed of four or more metallic elements mixed in an equimolar or near equimolar ratio [1]. The introduction of near-equiatomic multicomponent single phase high entropy alloys has changed the conventional alloy design process in which only one or two principal elements determine the material primary properties [2,3]. It was historically assumed that the presence of a high concentration of multiple alloying elements would embrittle the material by forming intermetallic compounds, and hence relatively little work was performed on alloys containing more than three major solute elements until one decade ago. Several compositions of HEAs or multicomponent alloys have been found to form ductile solid-solution structures involving face centered cubic (FCC) or body centered cubic (BCC) phases or mixtures of the two, instead of brittle intermetallic compounds [3–6]. In addition, their attractive physical and mechanical properties such as high strength, ductility, wear resistance, high temperature softening resistance and corrosion resistance make HEAs potential candidates for high temperature fission or fusion structural applications. Nonetheless, there is practically nothing known about their radiation resistance at elevated temperatures relevant for potential nuclear energy applications. It is hypothesized that the high configurational entropy might influence point defect recombination phenomena in irradiated materials by modifying the vacancy-interstitial recombination interaction distance, solute diffusivity, or other mechanisms, thereby producing different (superior or inferior) radiation stability compared to conventional single phase alloys.

Prior radiation effects studies on high entropy alloys have

* Corresponding author.
E-mail address: anantha.nimishakavi@mail.mcgill.ca (N.A.P.K. Kumar).

http://dx.doi.org/10.1016/j.actamat.2016.05.007
1359-6454/

examined only a partial subset of microstructural phenomena that might occur in these alloys due to displacement damage, with most of these prior studies performed at room temperature. Nagase et al., have investigated the irradiation-induced structural changes in nanocrystalline (~10 nm grain size) CoCuCrFeNi FCC HEA thin films (25 and 100 nm thick) under 2 MeV in-situ electron irradiation at 298 and 773 K by high voltage electron microscopy. It was shown that the HEA FCC phase exhibited generally good stability up to 40 displacements per atom (dpa) of irradiation at 298 K and 773 K (some phase decomposition to BCC and B2 phases occurred for doses above ~2 dpa, but this trend was also observed after thermal annealing at elevated temperatures without irradiation) [7]. A similar 2 MeV electron irradiation study at room temperature and 103 K on nanocrystalline (1–24 nm grain size) BCC Zr-Hf-Nb also reported moderate nanoscale precipitation with generally good stability of the BCC matrix phase up to ~40 dpa [8]. Since nanoscale grain sizes are known to inhibit radiation-induced solute segregation and radiation-induced phase decomposition [9], it is uncertain what role (if any) that concentrated compositional complexity might be playing to enhance phase stability in these studies. In addition, the relatively low knock-on atom energies associated with electron irradiation are not representative of the energetic displacement cascade conditions representative of fast neutron or energetic heavy ion irradiations. In general, phase stability during irradiation involves a competition between ballistic dissolution of precipitate embryos by energetic displacement cascades and coupled solute-defect radiation-enhanced diffusion to stimulate precipitate nucleation; therefore, the low primary knock-on atom energies associated with electron irradiation are difficult to extrapolate to energetic primary knock-on atom energies representative of nuclear energy applications. Another recent study on FCC-based AlxCoCrFeNi HEAs has reported good phase stability following heavy ion (3 MeV Au) irradiation at room temperature up to ~50 dpa [10]. However, since radiation-induced solute segregation and radiation-induced precipitation are generally only observed during irradiation at intermediate temperatures near 0.35–0.6 T_M, where T_M is the melting temperature [11–13], the applicability of these room temperature studies to elevated temperature (300–800 °C) nuclear energy systems is questionable. Overall, the recent studies on irradiated HEAs suggest good resistance to amorphization and good phase stability during room temperature irradiation [14–16], but these prior studies did not perform detailed microstructural or solute segregation (particularly grain boundary segregation) evaluations. In general, open questions include whether HEAs exhibit fundamentally different responses to irradiation compared to conventional metallic alloys, and whether they are viable candidates for nuclear energy applications (which involve a range of elevated irradiation temperatures, typically ~300 °C for light water reactors and 300–800 °C for fusion and Gen IV fission applications) [17].

In the current water-cooled nuclear fission reactors, austenitic (FCC) steels are widely used as a structural material, and high performance steels are considered to be essential for numerous proposed future nuclear energy systems, including sodium-cooled fast fission reactors and fusion reactor first-wall structures that require excellent radiation resistance to high doses of 100–200 displacements per atom (dpa) [17–19]. On the other hand, currently available austenitic stainless steels do not appear to exhibit sufficient radiation damage resistance for extended operation at elevated temperatures in next generation nuclear energy systems [17,18]. Radiation degradation of Fe-based austenitic steels is associated with several phenomena, including void swelling, irradiation-assisted stress corrosion cracking, decrease in fracture toughness and radiation-induced segregation (RIS). Of these, void swelling and RIS are two extremely important challenges for materials exposed to irradiation at elevated temperatures. The void swelling behavior of steels can cause unacceptable dimensional expansion and can lead to degradation of fracture toughness [17,20], whereas RIS can lead to phase instability, embrittlement, and stress corrosion cracking issues [11,21].

Radiation-induced segregation is a phenomenon in which the local alloy composition is altered by the coupled motion of solute with the vacancy or interstitial-type point defects in irradiated metals. This leads to enrichment or depletion of solute elements near point defect sinks such as grain boundaries, phase boundaries, dislocations and voids. The mechanisms controlling RIS in steels are associated with inverse Kirkendall (vacancy) effects and solute drag coupled with the diffusional flow of vacancies or interstitials [11,12,22]. A strong variation in RIS has been observed in austenitic Fe-Cr-Ni alloys with the change in irradiation temperature, flux, composition, and grain boundary type [22–24]. Although depletion of Cr is universally observed at grain boundaries in irradiated austenitic steels, the experimental observations on ferritic/martensitic (BCC) steels shows more complex behavior with either enrichment or depletion at the grain boundary depending on the detailed irradiation conditions [22,24–28]. A similar complexity in RIS was reported in Fe-Cr-Mn based austenitic steels. Although Cr depletion at sinks occurs in both Fe-Cr-Ni and Fe-Cr-Mn alloys, the segregation trend in Fe-Cr-Mn alloys is different due to the fact that Fe is predominantly enriched at the grain boundary sinks in Fe-Cr-Mn, while Ni enrichment is predominant in Fe-Cr-Ni alloys. Fe segregation often leads to phase instability or decomposition at higher irradiation temperatures. Therefore, although a clear trend of Mn depletion and Fe enrichment was seen in Fe-Cr-Mn alloys at lower irradiation temperatures, the behavior at higher irradiation temperatures is often unclear [29,30]. In recent years ab-initio calculations using density functional theory (DFT) have been used to examine the RIS behavior in austenitic and Fe-Cr-Ni alloys [31–33]. However, many uncertainties remain regarding the solute segregation behavior during irradiation, in particular the competition between interstitial vs. solute drag mechanisms [22,34,35]. In addition, very little is known about the influence of additional factors such as configurational entropy on the RIS behavior.

The key objective of the present study is to examine the extent of microstructural and mechanical changes produced by irradiation on a specific solid solution austenitic HEA compared to conventional Fe-Cr-Ni FCC alloys, in order to determine if HEAs might exhibit substantially different irradiation-induced responses such as RIS, radiation hardening, or void swelling. This work provides the initial examination of the fundamental irradiation behavior of an HEA material, thereby giving insight into the potential of this family of materials for nuclear applications.

2. Experimental

Many of the high entropy alloys studied to date contain Co, making them unfavorable for nuclear applications due to high neutron transmutation-induced radioactivity that can increase radiation shielding requirements during handling after neutron irradiation and can lead to undesirable increase in radiation exposures to workers during maintenance of nuclear power plants. In the present study, a novel 27%Fe-28%Ni-27%Mn-18%Cr (wt%) high entropy alloy has been synthesized [36]. The material was prepared by arc-melting a mixture of constituent metals of high purity. In general, the high entropy alloy should consist of approximately equimolar compositions in order to maximize configurational entropy. However, exploratory studies determined that the Fe-25%Ni-25%Mn-25%Cr alloy was not a single phase. The reduced Cr levels (compared to an equimolar composition) produced a single phase FCC structure as determined through X-ray diffraction and electron

microscopy. The cast bar was homogenized at 1200 °C for 48 h, then cold rolled and recrystallized at 900 °C for 4hr in a vacuum furnace to obtain fully recrystallized equiaxed microstructure with a grain size of ~35 μm (note this recrystallization time is longer than the 1 h time used for a companion study [36], resulting in a larger grain size, ~35 μm vs. ~15 μm in Ref. [36]). As shown in Fig. 1 and discussed elsewhere [36], the alloy exhibited good strength and ductility over a wide temperature range, with yield strength and total elongation smoothly varying from 450 MPa to 45% at −200 °C to 120 MPa and 12% at 800 °C. All of the specimens were mechanically polished down to 1 μm diamond lapping film prior to ion irradiation.

Ion irradiations were performed at two irradiation facilities; the University of Tennessee—Oak Ridge National Laboratory ion beam materials laboratory (IBML) and Texas A&M University Radiation effects facility (REF). Ion irradiation doses were computed by SRIM [37] assuming a displacement energy of 40 eV and following the recommendations of Stoller (quick Kinchin-Pease option) [38]. The calculated ion ranges for 3 MeV and 5.8 MeV Ni ions are ~1.07 and ~2.5 μm and mid-range dose is evaluated at a depth of ~0.5 and ~1 μm respectively. The damage and implanted ion profiles generated using SRIM are shown in Fig. 2. Microstructural and micro chemical characterization was mainly performed at mid-range depths (intermediate between the surface and peak damage regions) to minimize artifact effects associated with the surface sinks and implanted ions, respectively [39–41]. The 3 MeV Ni ion irradiations were performed to fluences of 4.2×10^{13}, 4.2×10^{14} and 4.2×10^{15} ions/cm^2 (0.03, 0.3 and 3 dpa midrange doses; cf. Fig. 2 and Table 1) at room temperature and 500 °C in the IBML at a test chamber pressure near or below 10^{-7} torr, and the 5.8 MeV Ni ion irradiations to fluences of 2.43×10^{15} and 2.43×10^{16} ions/cm^2 (1 and 10 dpa midrange doses; cf. Fig. 2 and Table 1) at temperatures 400, 500, 600, 700 °C were performed at REF at a nominal pressure below 10^{-6} torr. For the 3 MeV Ni ion irradiations, the particle fluxes were ~3.5×10^{11}/cm^2-s (2×10^{-4} dpa/s at midrange) at room temperature and ~3.5×10^{12}/cm^2-s (2×10^{-3} dpa/s at midrange) at 500 °C. For the 5.8 MeV Ni ions, the particle flux was ~6.5×10^{11}/cm^2-s (~3×10^{-4} dpa/s at midrange) at all temperatures. Due to in part to outgassing from the silver paste used to attach the specimens to the target holder, and also due to a vacuum leak in the target chamber during the elevated temperature irradiations, all the irradiations performed at the REF exhibited moderate surface contamination following irradiation. The contaminated layer formed on the sample surface was relatively non-uniform and the thickness ranged from ~100 nm in 400 °C to ~200 nm in 700 °C. Through energy dispersive spectrometry analysis, it was found that the contaminated layer is a Mn rich oxide. The selective oxidation of Mn in HEA coincided with Mn depletion under the oxide scale. The decrease in Mn concentration was most pronounced at the oxide-metal interface and recovers back to the bulk concentration beyond a temperature-dependent specimen depth. The near-surface depletion of Mn in the specimens were observed to a depth of ~0.2 μm at 400 °C, 0.4 μm at 500 °C, 1.5 μm at 600 °C and 2.2 μm at 700 °C. The decrease in Mn was accompanied by an increase in the matrix Fe and Ni concentration. Since microstructural analysis of these specimens was concentrated on the midrange region of ~1.2 μm from the irradiated surface, the Mn depletion may affect the quantitative results for the 600 and 700 °C irradiated specimens.

Hardness measurements on unirradiated and 3 MeV Ni ion-irradiated samples were performed at room temperature using a MTS XP nanoindenter. Hardness was not measured on the 5.8 MeV Ni ion irradiated samples due to the variability associated with the surface contamination layer in these samples. A Berkovich diamond indenter (3-sided pyramidal tip) was used for the tests. All the tests were performed in continuous stiffness measurement mode [42] with a constant loading rate $\dot{P}/P = 0.05$ s^{-1} and the maximum load applied was 150 mN. For good statistical analysis, each sample was indented with at least 16 to 25 indents, and the average of the results was used in the analysis. Hardness was measured as a function of depth from the point of contact of the nanoindenter with the surface to a depth of about 1800 nm. The hardness data within ~200 nm from the sample surface was discarded due to large data scatter associated with surface roughness. Since it is well known that the indentation hardness is sensitive to regions that are several times the indentation depth, the indentation transition depth between the near-surface ion damaged layer and underlying undamaged substrate was experimentally determined to be ~350 nm for all irradiation conditions by the method outlined by Nix and Gao [43]. Consequently, the hardness at an indenter depth of 300 nm was selected as the best condition that measured only the 3 MeV Ni ion irradiated region, without the large data scatter at shallower indentation depths (associated with surface roughness artifacts). Nanoindentation tests were not performed on the 5.8 MeV Ni ion irradiated specimens as the non-uniform contamination layer, formed due to poor vacuum during irradiation, would influence the determination of specimen contact area, and would therefore cause errors in the measurement of hardness and modulus.

Conventional X-ray diffraction measurements were performed on the as-fabricated Fe-Ni-Mn-Cr HEA bulk material with a copper tube (K_α wavelength $\lambda = 1.5406$ Å) at room temperature at an

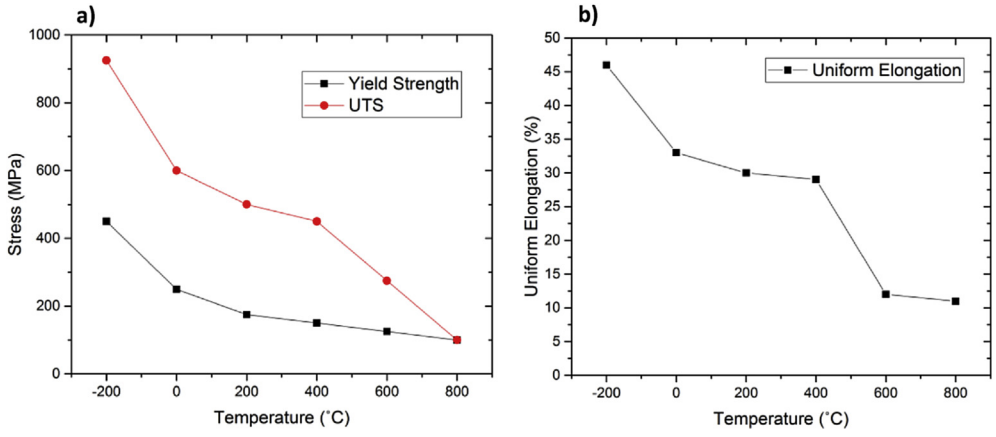

Fig. 1. Temperature dependence of uniaxial tensile properties of Fe-Ni-Mn-Cr HEA a) 0.2% Yield and ultimate tensile strength b) Uniform elongation.

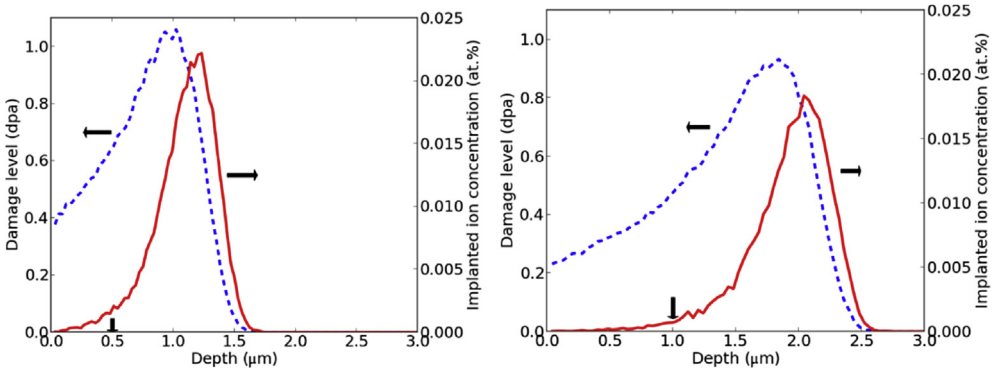

Fig. 2. SRIM plots showing the calculated damage (dashed line) and implanted ion profiles (solid line) of 3 MeV (left) and 5.8 MeV (right) Ni ions in 27%Fe-28%Ni-27%Mn-18%Cr, normalized to an ion fluence of 10^{15} ions/cm^2. The vertical arrows indicate the depth where the midrange dose is evaluated.

Table 1
Summary of ion irradiation conditions for the Fe-28%Ni-27%-Mn-18%Cr high entropy alloy. All doses refer to midrange values (depths of 0.5 and 1 μm for 3 and 5.8 MeV Ni ions, respectively).

3 MeV Ni ions	5.8 MeV Ni ions
0.03 dpa at Room temp.	1 dpa at 500 °C
0.3 dpa at Room temp.	10 dpa at 400 °C
0.3 dpa at 500 °C	10 dpa at 500 °C
3 dpa at 500 °C	10 dpa at 600 °C
	10 dpa at 700 °C

accelerating voltage and current of 40 kV and 40 mA. The interval between each acquisition was 0.02° and the step time was 1s; XRD spectra for HEA samples recrystallized by 1 h anneal at 900 °C are described in Ref. [36]. A PANalytical Xpert diffractometer with a MoK$_\alpha$ ($\lambda = 0.70932$ Å) target operated at 45 kV and 40 mA with a scan rate of ~1°/min (0.02° step size) at room temperature was used to perform grazing incidence X-ray measurements on the unirradiated and 3 MeV Ni ion irradiated samples. The incident beam was fixed at 2° relative to the sample surface, so the maximum penetration depth was <2 μm. All scans used 2 mm adjustable slits and 2° anti-scatter slit so that the same portion of the sample was always in the X-ray beam throughout the scan. The detectable phase limit of the diffractometer for this glancing angle experimental configuration is ≈ 3 wt% (mainly determined by instrument-related parameters since the HEA specimen exhibited low scattering); therefore, minor phase volumes <3% were not detectable.

Microstructural characterization included scanning electron microscopy (SEM) and transmission electron microscopy (TEM). A JOEL 6500F SEM equipped with dispersive x-ray spectrometry (EDS) X-ray detector was used to analyze the dark spots on the HEA specimens. For EDS work, the SEM accelerating voltage was 20 kV; the working distance was 10 mm. Cross-section transmission electron microscopy (TEM) specimens from the irradiated samples were prepared using a focus ion beam (FIB) (FEI Quanta 3D 200i) system with Ga^+ ions. The ion energy at the main thinning step was 30 keV, and during the later stages of thinning, the energy was progressively reduced to 8, 5 and 2 keV with the final thinning at a foil thickness of ~100 nm performed with a current of 27 pA. In order to further minimize the unwanted FIB surface damage caused by Ga^+ ions, a low voltage argon ion polishing system (Fischione NanoMill-model 1040) was subsequently used for creating high quality TEM specimens. A very low voltage and current of 900 eV and 90 pA were used at this stage of TEM specimen preparation. As a final step, a Fischione Plasma Cleaner (Model 1020) was used to remove carbonaceous contamination from the TEM specimen. A Philips CM200 FEG (field emission gun) TEM/scanning transmission electron microscope (STEM) that produces a probe of 1.4 nm at 200-kV operating voltage was used to examine the irradiation damage in the specimens. Compositional changes across the grain boundaries of irradiated specimens were analyzed using a Talos F200X high-resolution STEM microscope equipped with SuperX EDS system with four silicon drift detectors (SDDs) with total active area of 120 mm^2. For this work, a probe of <1 nm at 200 kV was used and an average count rate ~10^5 X-rays/s was obtained from thin HEA specimens. Elemental spectrum images on specimen area ~1300 × ~1300 nm were collected for ~360s. EDS spectrum images were acquired and analyzed using Bruker Esprit software on at least two representative high angle grain boundaries for each high temperature (400–700 °C) irradiated sample.

3. Results and discussion

Metallographic examination of the as-fabricated Fe-Ni-Mn-Cr HEA specimen revealed an equiaxed grain structure with a few annealing twins (see Fig. 3). The average grain size of the as-fabricated alloy was ≈35 μm, based on line intercept method measurements of SEM images. Very few observable precipitates (black spots in Fig. 3a,b) were seen in the backscattered electron images. EDS analysis indicated the observed precipitates are oxides rich in Cr and Mn. X-ray diffraction measurement on the bulk material after final heat-treatment showed a single phase polycrystalline structure without any second phase. This indicates that the amount of second phase in current HEA is less the detection limit of 3 wt%.

Grazing incidence XRD measurements were performed on the unirradiated and 3 MeV Ni ion irradiated samples to investigate potential phase and structural changes. As shown in Fig. 4, the samples remained fully crystalline and retained their original FCC phase, with no detectable second phase observed as a function of irradiation temperature and dose up to 0.3 or 3 dpa at room temperature or 500 °C, respectively. The variability in peak intensity is believed to be associated with moderate texture in the samples (different orientation with respect to the glancing x-ray beam). The cause of the slight shoulders in some of the peaks is uncertain, particularly since they are present in some of the unirradiated peaks (~19, 32, 38°) whereas they were not observed in the XRD investigation of the nominally identical HEA specimens in ref. [36]. No significant second phases beyond a few isolated oxide particles were observed in the TEM and EDS spectrum mapping analyses of the 5.8 MeV Ni ion irradiated samples, including the samples irradiated to 10 dpa at 400–700 °C. As a summary, TEM and XRD characterization on the ion irradiated samples subjected to doses

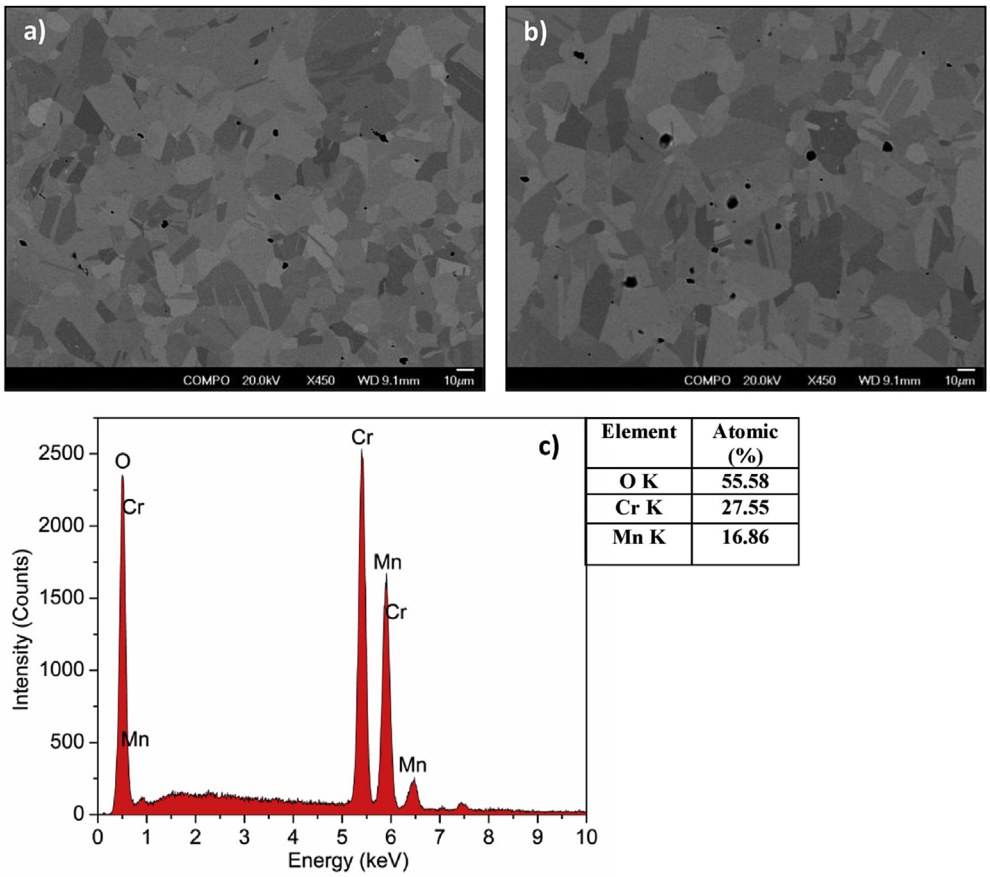

Element	Atomic (%)
O K	55.58
Cr K	27.55
Mn K	16.86

Fig. 3. a), b) SEM-BSE micrographs of Fe-Ni-Mn-Cr HEA control sample (Note: Black spots in the micrographs are Cr-Mn rich precipitates c) EDS plot of second phase precipitates. (Insert table is the composition of the precipitate).

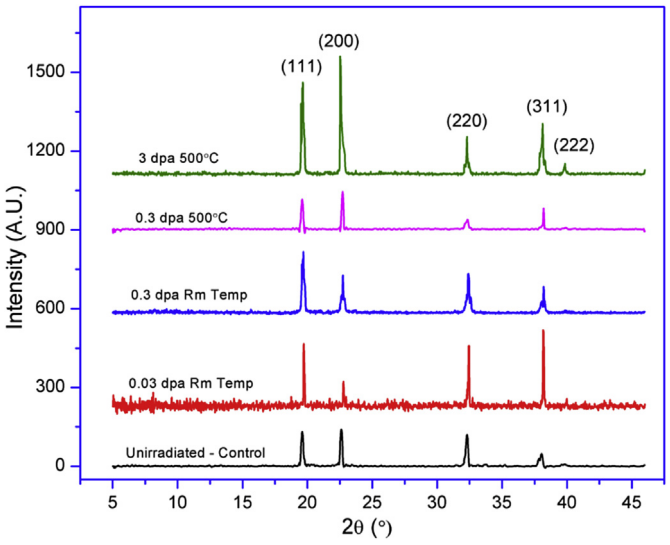

Fig. 4. Glancing incidence XRD patterns of the unirradiated and 3 MeV Ni ion irradiated Fe-Ni-Mn-Cr HEA samples exposed to different irradiation conditions.

up to 10 dpa and temperatures between room temperature and 700 °C showed a stable FCC phase with a low density of Cr and Mn rich oxide precipitates.

3.1. Dislocation loops and network dislocations

Fine scale dislocation loops with diameters ranging from 1 to 10 nm dominated the visible defect microstructure at 400–700 °C. An even high density of slightly smaller loops was observed following irradiation to 0.03 and 0.3 dpa at room temperature. Fig. 5a shows a representative weak-beam dark field image of the dislocation structure of an ion irradiated Fe-Ni-Mn-Cr HEA specimen at 10 dpa, 700 °C taken with foil orientation near the ⟨110⟩ zone axis. Fig. 5b summarizes the temperature dependence of the measured dislocation loop diameter after 10 dpa irradiation at 400–700 °C. The loop sizes were determined by measuring the longest axis of visible loops taken from weak beam dark field micrographs. On an average 75–100 loop diameters were considered to obtain the average loop size. The dislocation loop volumetric density was determined from the slope of the measured areal loop density versus foil thickness; this method eliminates errors associated with possible FIB surface damage artifacts or near-surface regions that are denuded of dislocation loops [44]. Table 2 summarizes the average loop diameter (d) and loop volumetric density (N) in the HEA samples for the different irradiation doses and temperatures. A slight increase in loop size and decrease in loop density is observed with increasing irradiation temperature for doses above 0.3 dpa. The increase in dislocation loop size with increasing temperature is relatively modest (from 4 to 5.5 nm as temperature is increased from 400 to 700 °C for a dose of 10 dpa). Loop density appears to nearly saturate after exposure to a dose of 0.3 dpa at 500 °C, which is consistent with prior ion irradiation studies on Fe-Cr-Ni alloys near 500 °C [45]. It should be noted that

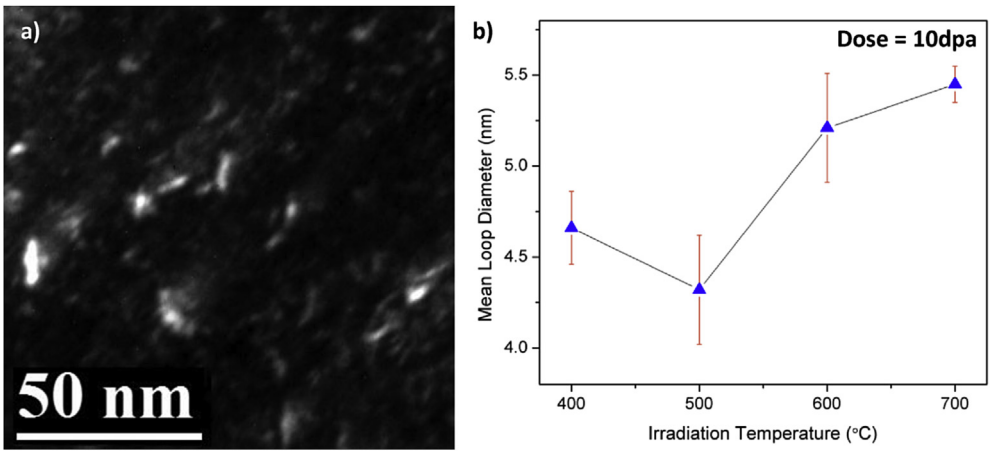

Fig. 5. a) Dislocation loops and small defect clusters in weak beam dark field image of 10 dpa 700 °C irradiated specimen g,3 g, (g = 200), b) Change in dislocation loop size with respect to irradiation temperature.

Table 2
Summary of measured dislocation loop parameters in the ion irradiated Fe-Ni-Mn-Cr HEA samples.

Temperature (°C)	Dose (dpa)	Mean loop diameter (nm)	Loop density (m^{-3})
Room Temp	0.03	2.98	7.3×10^{22}
Room Temp	0.3	3.23	1.5×10^{23}
400	10	4.66	1.9×10^{22}
500	3	4.13	7.1×10^{21}
500	10	4.32	9.4×10^{21}
600	10	5.21	6.7×10^{21}
700	10	5.45	4.3×10^{21}

the concentration of point defects retained in visible defect clusters in the irradiated HEA samples ($N\pi d^2 b/4$, where b~0.2 nm) is ~30 atomic parts per million, i.e., nearly 6 orders of magnitude less than the integrated concentration of point defects produced by the 10 dpa irradiations.

Fig. 6 compares the temperature-dependent dislocation loop densities for the Fe-Ni-Mn-Cr HEA with previously reported data [45–58] on ion-irradiated Fe-Cr-Ni alloys. At low temperatures

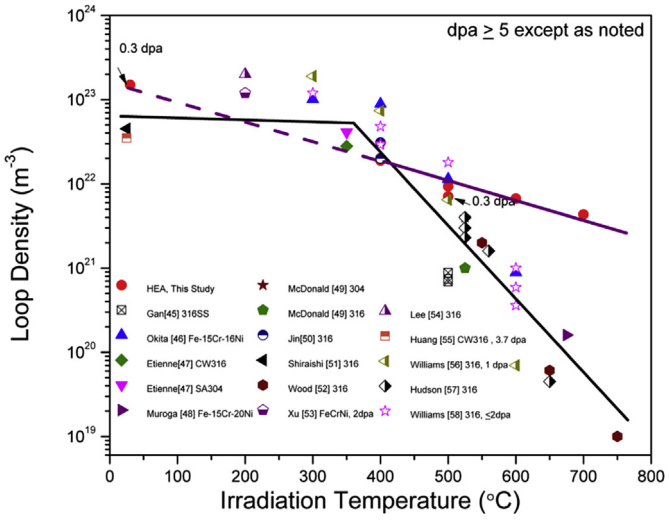

Fig. 6. Effect of ion irradiation temperature on dislocation loop density for Fe-Ni-Mn-Cr HEA compared to conventional Fe-Cr-Ni austenitic alloys [45–58] irradiated at comparable doses and damage rates. The drawn lines are intended as guides for the reader's eye.

between room temperature and ~400 °C, the HEA and conventional Fe-Cr-Ni loop densities are comparable and nearly independent of dose (>0.3 dpa) and temperature with values near ~10^{23} m^{-3}. For irradiation temperatures above 400 °C, the loop densities monotonically decrease and loop sizes (not plotted in Fig. 6) monotonically increase with increasing temperature. However, the temperature dependence at 400–700 °C is less pronounced and the overall loop densities are significantly higher in the irradiated HEA compared to the reported dislocation loop densities of Fe-Cr-Ni alloys irradiated under similar conditions; the HEA loop density is nearly 100 times larger than that measured in conventional Fe-Cr-Ni alloys irradiated at 700 °C. The corresponding loop sizes for the HEA specimens are much smaller than reported for Fe-Cr-Ni alloys [45,57,58] at irradiation temperatures of 400–700 °C. For example, Hudson [57] reported the average loop diameter in Ni ion irradiated Type 316 stainless steel increased from ~33 nm at 525 °C to 110 nm at 650 °C after irradiation near 10 dpa and Williams [58] reported loop diameters in 1 dpa Ni ion irradiated Type 316 stainless steel increased from ~5 nm at 400 °C to ~30 nm at 600 °C, whereas the ion irradiated HEA average loop diameter did not exceed 6 nm for irradiation temperatures up to 700 °C (Fig. 5b). A slight variation in reported defect cluster density (particularly for irradiation temperatures ≤300 °C) could be due to the fact that some authors separated the "black spots" (small defect clusters) and dislocation loops, whereas in the current HEA study both black spots and dislocation loop are treated as dislocation loops due to their comparable sizes. In addition, if the imaging of small loops is done in thick (>150 nm) foil regions, lower loop density (up to a factor of ~2) is observed due to poor contrast of small (~2 nm) loops and overlap effects [44]. In this study, all the observations were made in relatively thin foils (thickness of 60–80 nm, measured with two-beam convergent beam electron diffraction pattern (CBED) method). However, neither "blackspot" differentiation nor

thick foil effects can explain the ~100× difference in loop density for HEA vs conventional austenitic alloys at 700 °C and the pronounced difference in HEA vs. conventional alloy loop size at high temperatures.

A network dislocation density of ~10^{13}–10^{14} m^{-2} was measured in the annealed unirradiated Fe-Ni-Mn-Cr HEA using standard line intercept methods on bright field TEM images under dynamic contrast conditions. No change in network dislocation density with irradiation was observed for any irradiation condition, which indicates that the dislocation loops haven't grown enough to coalesce and form network dislocations at any of the investigated irradiation conditions. Relatively constant defect cluster (dislocation loop) density was also observed for the high temperature (400–700 °C) irradiated specimens. In conventional Fe-Cr-Ni alloys, the increase in irradiation temperature above 400 °C results in a pronounced decrease in loop density and an increase in loop diameter due to an increase in diffusion rate of interstitials and vacancies [57–60]. However, the nearly constant dislocation loop density (only a factor of 5 decrease between 400 and 700 °C) and limited increase in loop size (17% increase in size between 400 and 700 °C, Table 2) in the ion irradiated HEA specimens suggest that the diffusion kinetics in HEAs are more sluggish than in conventional Fe-Cr-Ni alloys. In addition, the smaller loop size in HEA suggests that only a small fraction of the produced point defects are eventually trapped in the loops and recombination of vacancies and interstitials is the dominant recovery process in the HEAs. Although the concentration of point defects contained in visible dislocation loops ($N\pi d^2b/4$) at an ion irradiation temperature of 500 °C is only about a factor of 3 lower in the HEA than conventional Fe-Cr-Ni alloys, the suppressed network dislocation density in the irradiated HEA samples (~10^{13}–10^{14} m^{-2} versus ~5 × 10^{14} m^{-2} in ion-irradiated Type 316 stainless steel at ~500–650 °C [57,58]) should provide somewhat superior resistance to void swelling, irradiation creep, etc. according to kinetic rate theory considerations.

3.2. Voids

Voids are commonly formed in irradiated single phase materials for doses above ~1 dpa at temperatures where vacancies are mobile, due to accumulation of radiation-induced vacancies into stable cavities [61]. Void swelling in Fe-Cr-Ni alloys at elevated temperatures (>400 °C) has a significant deleterious impact on allowable lifetime and reactor operations [17,62–68]. Earlier studies have shown that overall swelling of Fe-Cr-Ni alloys can be modified by varying the Ni and Cr concentration [63,68], but in general void formation is expected in conventional Fe-Cr-Ni alloys for ion irradiation doses above 1–10 dpa at 450–650 °C [45,46,57,69]. Fig. 7 shows the over- and under-focused TEM micrographs of an Fe-Ni-Mn-Cr HEA specimen irradiated at 700 °C to 10 dpa. The search for void formation was performed in the midrange damage regions (~1 μm for the 5.8 MeV Ni ion irradiated samples) in order to minimize void swelling suppression effects associated with injected ions near the peak damage region (~2 μm) or the high point defect sink effects associated with the irradiated sample surface [39,40]. In general a void density of 10^{20}–10^{22} per m^3 and a swelling of 0.1–2.5% have been reported in conventional austenitic steels under similar ion irradiation conditions of 450–700 °C and ~10 dpa [45,46,56,57]. In contrast, the HEA samples showed no detectable void formation at any of the ion irradiation conditions in this study. The fact that no voids are observed after irradiation to midrange doses of 10 dpa at 400–700 °C indicates that the HEA has better swelling resistance than conventional austenitic Fe-Cr-Ni or Fe-Cr-Mn alloys [70]. Although nickel is the slowest diffusing element compared to Fe, Cr and Mn, it is thought to raise the effective vacancy diffusion coefficient thereby decreasing the void nucleation rate [71]. Therefore the composition (higher Ni content) of the HEA could have played a major role, but complete void suppression might not be solely ascribed to higher Ni content, as several other factors, such as high configurational entropy effect, sluggish diffusion effect and self-healing (enhanced vacancy-interstitial spontaneous recombination radii) effect could play a significant role in the observed resistance to void formation of HEAs up to 10 dpa over a wide range of temperatures.

3.3. Radiation induced segregation (RIS)

Fig. 8 shows the scanning transmission electron microscopy (STEM) micrographs of the Fe-Ni-Mn-Cr HEA specimens exposed to different irradiation conditions and the integrated line profiles that were extracted from area-scans performed across the grain boundaries. Random high angle grain boundaries were selected for segregation measurements, as these boundaries typically exhibit higher solute segregation than low angle boundaries [72,73]. Irradiations from room temperature up to 500 °C and 1 dpa did not show any measurable segregation detectable by Talos SuperX SSD detectors. Higher dose (10 dpa) irradiations at temperatures of 500, 600 and 700 °C showed Ni enrichment at grain boundaries, while Fe, Cr and Mn were depleted near the grain boundaries. The typical full width half maximum extent of the solute segregation region adjacent to the grain boundaries was ≤100 nm and was symmetrical on either side of the grain boundary. In the samples irradiated at 600 and 700 °C where Mn surface oxidation was accompanied by a decrease in the Mn matrix concentration from ~27 at.% to ≤16 at.%, the quantitative magnitude of the radiation induced segregation (RIS) may be affected by the matrix compositional changes (reduced Mn and increased Fe and Ni). However, the qualitative observed RIS trends are expected to be valid.

In general, the RIS in Fe-Cr-Mn or Fe-Cr-Ni alloys can be explained by either of two mechanisms; inverse Kirkendall effect [74–76] and solute drag effect [77,78]. Both the mechanisms can promote same segregation effect (e.g., for the inverse Kirkendall mechanism where Ni enriches because it is a slower diffusing oversized atom and Cr or Mn depletes because they are faster diffusing undersized atoms). A summary of both mechanisms can be found elsewhere [12,13]. In general, prior experimental measurements and model predictions for conventional Fe-Cr-Ni alloys suggest that significant RIS is observable at doses of ~0.1–1 dpa, and a tendency toward saturation occurs at higher doses (i.e., relatively small additional RIS occurs at higher doses) [79]. Overall, the grain boundary segregation trends observed in the examined HEA samples are qualitatively similar but less pronounced in magnitude compared to the behavior seen in austenitic stainless steels, where Ni enrichment and Cr and Mn depletion at grain boundaries have been reported following irradiation at intermediate temperatures in numerous prior studies [22,62,68,80].

Fig. 8 (e, f) shows the experimentally observed radiation induced segregation profiles at high angle grain boundaries in the Fe-Ni-Mn-Cr HEA samples that were ion irradiated to a dose of 10 dpa at 400 and 600 °C. Negligible solute segregation is observed at 400 °C, whereas measurable RIS is observed for Ni, Fe and Cr solutes at 600 °C with a ~90 nm typical full width half maximum segregation profile adjacent to the grain boundary. It is worth noting that this RIS width is significantly larger than the ~5–40 nm widths observed in conventional Fe-Cr-Ni alloys ion irradiated near 280 °C [9,11,21,81] and 520 °C [81–83], respectively. The measured amount of Ni enrichment or Cr depletion at the irradiated HEA grain boundary is significantly lower (by a factor of two or more) than that in austenitic steels under similar heavy ion irradiation dose rates and temperatures. For example, conventional 316 SS irradiated with Fe ions at 350 °C to a dose of 10 dpa showed ~17 at%

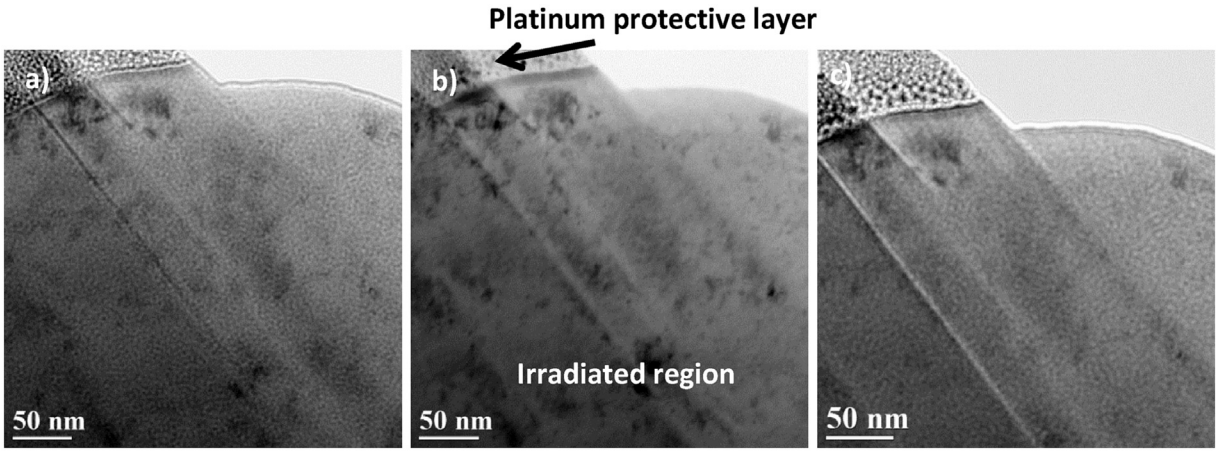

Fig. 7. Bright field TEM image series from Fe-Ni-Mn-Cr HEA alloy a) over-focus, b) focus c) under-focus, showing that no voids are observed in the specimen irradiated at 700 °C, 10 dpa.

enrichment in Ni concentration and ~12 at% depletion in Cr concentration [9], and 6–8 at% Cr depletion was reported in 304 SS and 316 SS after Ni ion irradiation at 500 °C to 5 dpa [83]. Similarly, the Cr depletion in 304 SS grain boundaries after 400 keV He ion irradiation to 3 to 10 dpa at 300, 400 and 500 °C was 3, 11.5 and 13.5 at%, respectively and the corresponding Ni enrichment was ~4, 13 and 19 at%, respectively [81]. However, in the current HEA, a maximum of ~7 at% Ni enrichment and ~3 at% Cr depletion was observed in the specimen irradiated to 10 dpa at 600 °C, with <1% solute segregation observed after 10 dpa at 400 °C. The other HEA elements (Mn and Fe) exhibited $\leq$ 3 at% grain boundary solute depletion compared to the matrix concentration after 10 dpa at 600 °C.

Earlier experiments on simple Fe-Cr-Ni and Fe-Cr-Mn ternaries alloys have shown that the alloy composition plays a significant role in its segregation behavior [18,79,84,85]. The diffusivities of elements such as Fe, Cr and Ni vary with the alloy composition, leading to dissimilar segregation at the grain boundaries [86]. Therefore, it is not surprising the investigated Fe-Ni-Mn-Cr HEA with higher concentrations of Ni, Mn and Cr could have a significant influence on its segregation behavior. The observed suppression of Cr depletion in the irradiated HEA compared to conventional Fe-Cr-Ni alloys and austenitic stainless steels could be due to the increase in bulk nickel concentration for the HEA [23,79,87]. The potential complexity in RIS behavior is also illustrated by previous grain boundary RIS results for Fe-Cr-Mn austenitic alloys. Contrary to current observations for the HEA and for low Mn alloys (moderate Mn depletion or no change compared to matrix concentration), Mn enrichment at grain boundaries was reported after irradiation for higher Mn content alloys [88]. Nevertheless, it is important to note that, unlike conventional alloys, in HEAs there is no solvent element that dominates the composition of the solid solution. Therefore, the influence of other effects, such as competing solute RIS kinetics, high entropy and severe lattice distortion, which are less pronounced in many conventional alloys, could increase the complexity of RIS processes in HEAs.

3.3.1. Temperature dependence of RIS

The temperature dependence of grain boundary RIS in the Fe-Ni-Mn-Cr HEA samples irradiated to a constant dose of 10 dpa was studied at irradiation temperatures ranging from 400 to 700 °C. Fig. 9 shows the normalized composition profiles adjacent to high angle grain boundaries for each solute element obtained from the SuperX EDS area scans as a function of temperature (i.e, the position-dependent solute concentration is normalized to the measured matrix concentration far from the grain boundary). This scaling with matrix solute concentration adjusts for the matrix Mn depletion and slight enhancement in Fe and Ni matrix concentrations of the HEA samples irradiated at 600 and 700 °C due to surface oxidation effects. The spatial width of the measured solute segregation profile near the grain boundaries was $\leq$100 nm at all irradiation temperatures. In most cases, the observed RIS profile exhibited a simple symmetric bell-shaped spatial dependence, although the Fe and Cr profiles for the 500 °C irradiation condition exhibits a slight deviation to a "W" shaped profile that has been previously reported in low dose (~1 dpa) RIS studies on austenitic stainless steels [21].

Fig. 10 summarizes the irradiation temperature dependence of the grain boundary solute concentrations (normalized to the bulk matrix solute levels) in the Fe-Ni-Mn-Cr HEA after 10 dpa ion irradiation. The RIS behavior for a proton irradiated conventional Fe-Cr-Ni alloy is also shown for comparison. No significant solute segregation at grain boundaries was observed at 400 °C in the irradiated HEA. Small amounts of Ni enrichment and Cr, Fe and Mn depletion were observed at temperatures between 500 °C and 700 °C. The magnitude of the RIS was most pronounced for Ni and was smallest for Cr and Fe solutes. Maximum Ni enrichment and Cr depletion was recorded at 600 °C. As the temperature increases to 700 °C, the amount of solute segregation is reduced compared to 600 °C. The decrease in RIS at 700 °C can be attributed to increase in point defect mobility with temperature, which will in turn induce back-diffusion for all solutes thus reducing the spatial concentration gradient near the grain boundaries [11–13,79]. At a given irradiation dose, the segregation peaks at intermediate temperatures and falls off at both higher and lower temperatures. According to existing RIS models, the observation of maximized RIS in the irradiated HEA near 600 °C is consistent with dominance of point defect recombination at low temperatures and high back diffusion at high temperatures.

Comparison of the radiation induced solute segregation results of the Fe-Ni-Mn-Cr HEA and a conventional Fe-Cr-Ni alloy in Fig. 10 indicates that the maximum segregation occurs at a higher temperature in the HEA. Generally, in conventional Fe-Cr-Ni austenitic alloys, maximum radiation induced solute segregation occurs at intermediate temperatures of 300 °C–500 °C, depending on specific alloy composition, dose rate and other irradiation parameters [79,84,85]. However in the current HEA, no RIS was detected at 400 °C and peak segregation was observed at 600 °C, indicating the

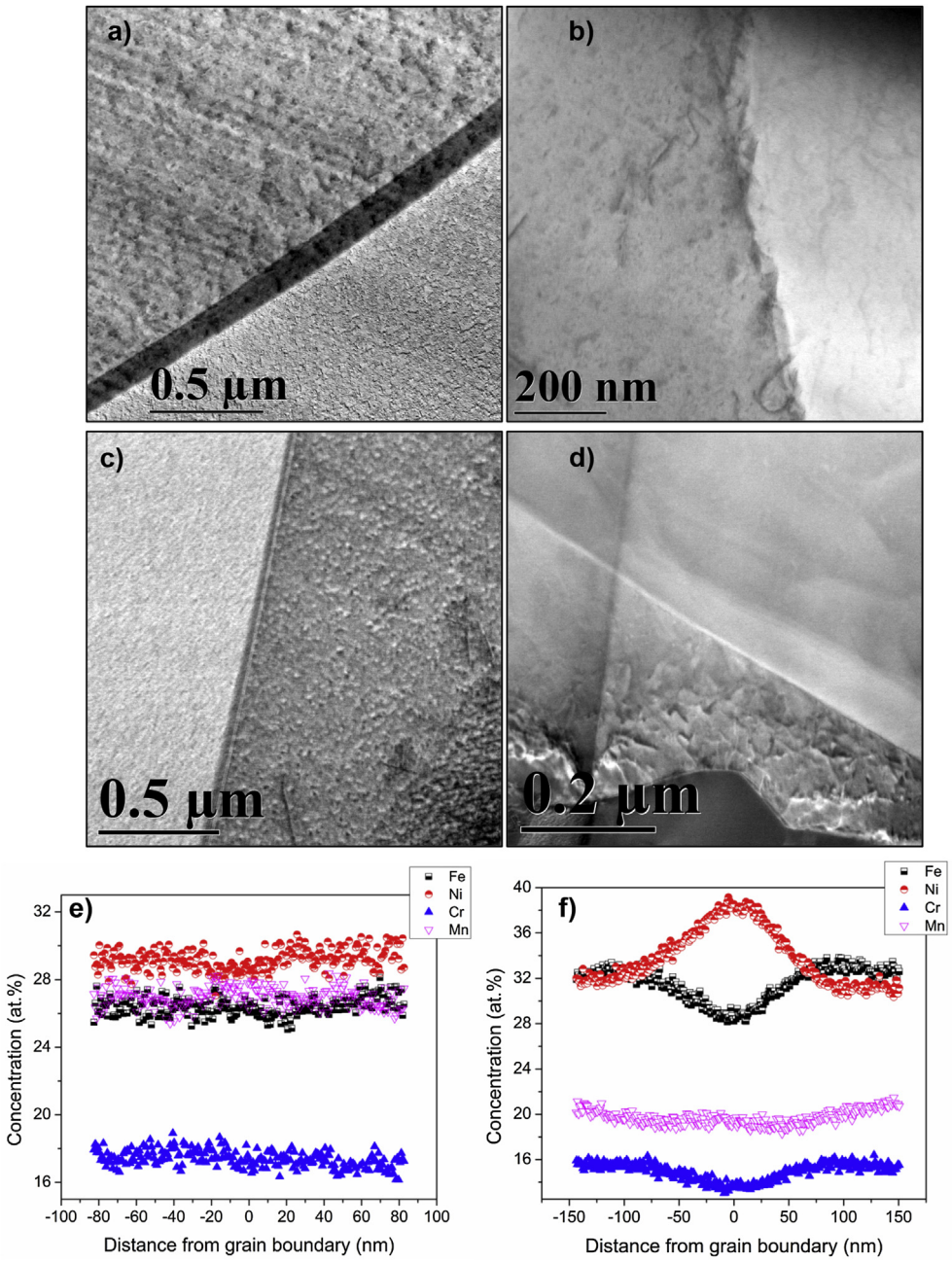

Fig. 8. STEM micrographs showing Fe-Ni-Mn-Cr HEA grain boundaries of a) control sample, b) 0.03 dpa RT c) 0.3dpa RT d) 10 dpa 700 °C. STEM/EDS grain boundary composition profiles are also shown for e) 10 dpa 400 °C and f) 10 dpa 600 °C specimens.

possibility of sluggish diffusion kinetics in Fe-Ni-Mn-Cr HEAs compared to conventional austenitic Fe-Cr-Ni alloys. The possibility of relatively low solute diffusivity in HEA alloys is supported by the recent study on Co-Cr-Fe-Mn-Ni high entropy alloy, where it was reported that the HEA showed larger fluctuation in lattice potential sites, which resulted in the presence of abundant low-energy lattice potential sites that would thereby lower the diffusion kinetics of solute atoms [89]. An alternative explanation for the higher irradiation temperature for peak RIS in the HEA is due to the 200X higher dose rate (3×10^{-4} dpa/s vs. 7×10^{-6} dpa/s for the proton irradiated conventional alloys in Fig. 10), which would be expected to shift the peak segregation to higher temperature [12,13]. Further follow-on work is also needed to determine if the matrix Mn depletion and slight enhancement in Fe and Ni matrix solute concentrations associated with the observed surface oxidation at 600 and 700 °C have a significant impact on the overall observed RIS trends in the Fe-Ni-Mn-Cr HEA; if the solute diffusivity is indeed suppressed in the near-equiatomic HEA, the modification in the HEA matrix solute composition at 600 and 700 °C to unequal solute concentrations could be expected to have an effect on solute diffusivities. In any case the quantitatively lower amount of radiation-induced solute segregation in Fe-Ni-Mn-Cr HEA over the broad temperature range of 400–700 °C indicates good RIS resistance of this material.

3.4. Hardness

Nanoindentation hardness is a useful tool to monitor

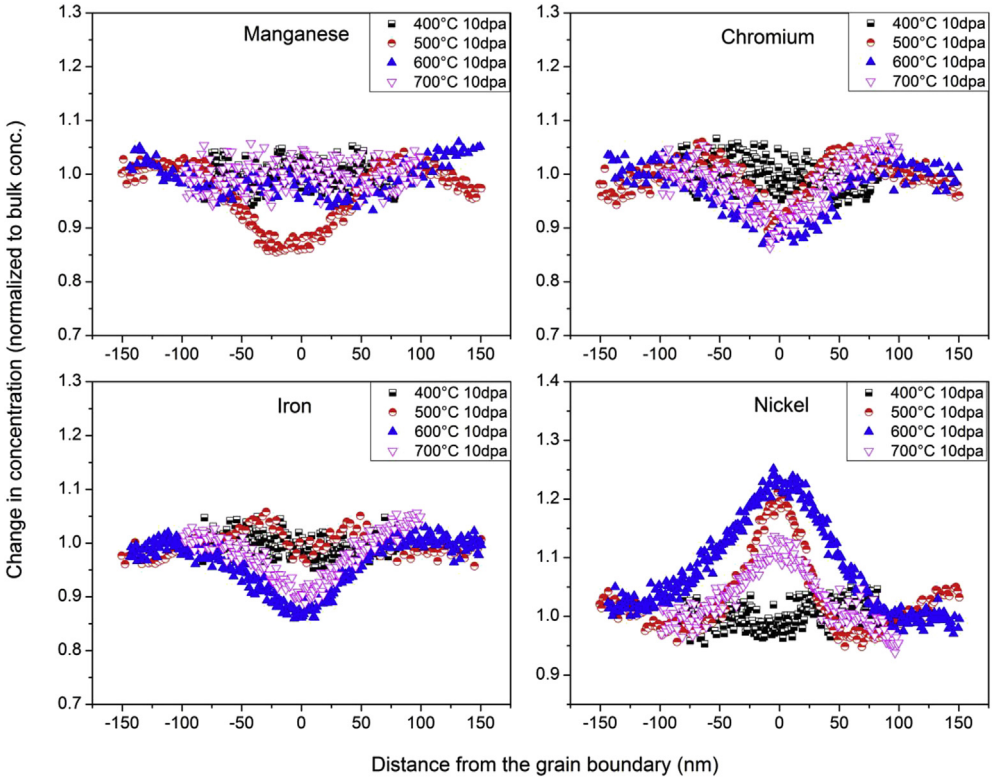

Fig. 9. Radiation-Induced Segregation: Change in concentrations at the grain boundary of individual element with respect to irradiation temperature.

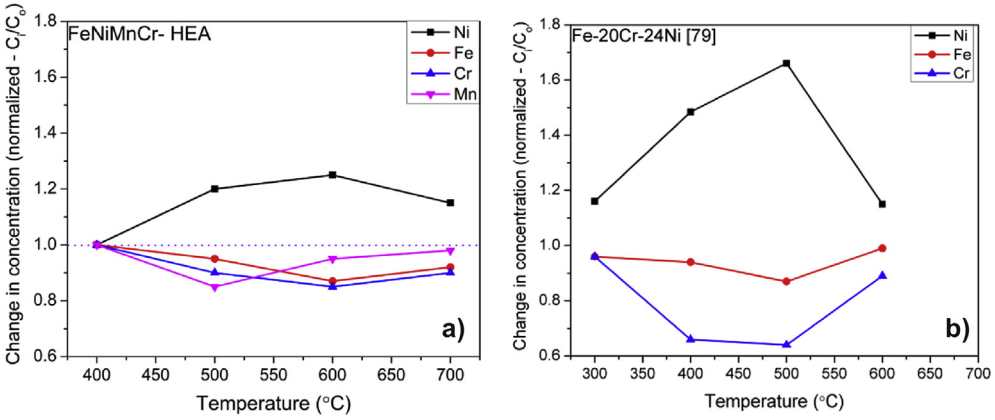

Fig. 10. Grain boundary solute segregation plotted as a function of irradiation temperature for a) Fe-Ni-Mn-Cr HEA in this study, and b) Fe-20Cr-24Ni irradiated with 3.2 MeV protons to a damage level of 0.1–3 dpa [79].

mechanical property changes in the small affected regions associated with ion irradiated samples. The normalized (irradiated to nonirradiated) depth-dependent hardness values of the irradiated Fe-Ni-Mn-Cr HEA samples are shown in Fig. 11. Since the elastic stress fields beneath the indenter are sensitive to microstructural features that are up to ~10 times the indenter depth, the maximum extent of the near-surface ion irradiated region that was unaffected by the underlying (softer) unirradiated substrate was determined using the method outlined by Nix and Gao [43] to correspond to an indenter depth of ~350 nm. The near-surface nanoindentation hardness data were found to exhibit large scatter due to the influence of surface irregularities, etc. Therefore, quantitative analysis of the nanoindentation hardness of the ion irradiated specimens used indenter depths from ~200 to 350 nm. The hardness in the ion irradiated region of the HEA samples increased rapidly with increasing dose at room temperature, from ~35% higher than the unirradiated value at 0.03 dpa to approximately 80% above the unirradiated hardness at 0.3 dpa. A similar increase in hardness was reported in Type 316 austenitic stainless steel ion irradiated to 0.6 and 3.7 dpa at room temperature [55]. The increase in the irradiated HEA hardness was less pronounced for irradiations at 500 °C, with values of 10–15% increase at 0.3 dpa and ~18% increase at 3 dpa.

High hardness of low-temperature irradiated specimens can be explained with commonly accepted models proposed by Orowan and Seeger [44,90,91]. In these models, the presence of irradiation defect clusters such as dislocation loops will increase the hardness of the material by acting as obstacles to the glide of dislocations.

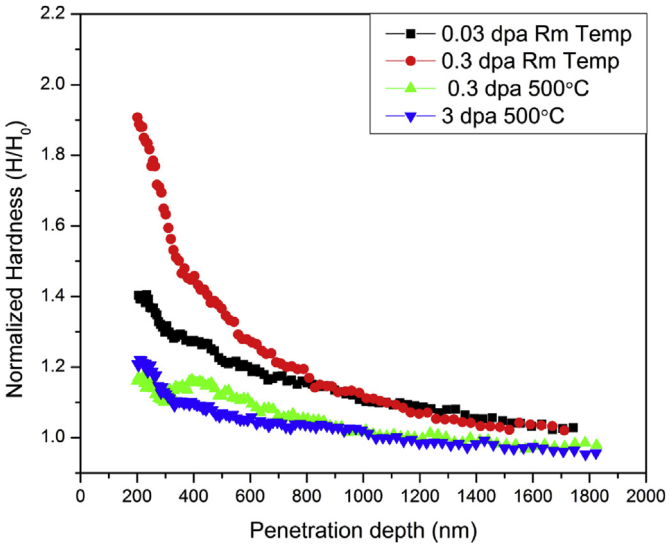

Fig. 11. Variation of hardness (normalized to unirradiated hardness) with indenter depth for Fe-Ni-Mn-Cr HEA specimens irradiated with 3 MeV Ni ions.

Similarly, the smaller increase in hardness of high temperature irradiated specimens containing a lower density of loops can be explained with the same model. For instance, the specimen irradiated to a dose of 0.3 dpa at room temperature had a loop density of 1.54×10^{23} m^{-3}, whereas the specimen subjected to same dose but irradiated at 500 °C showed a drastic drop in loop density of 7.13×10^{21} m^{-3} with only a slightly larger average loop size. Therefore, the change in defect structure itself can explain the reduced hardening of the HEA material at higher irradiation temperature. In order to quantify the contribution of dislocation loops on hardening in the irradiated HEA samples, the measured hardness is compared in the following with the predictions from the well-known dispersed barrier-hardening (DBH) model (see Equation (1)) [44,91].

$$\Delta\sigma_y = M\alpha\mu b\sqrt{(Nd)} \tag{1}$$

where $\Delta\sigma_y$ is the yield strength increase, M is the Taylor factor (3.06 for equiaxed BCC and FCC metals), α is the barrier strength factor, μ is the shear modulus, b is the Burgers vector of the gliding dislocations, N is the defect cluster density and d is the cluster diameter. Using the shear modulus of austenitic steels 77 GPa, α~0.4 (for strong obstacles such as dislocation loops) [92,93] and glide dislocation Burgers vector in austenitic steel $(a_0/2)\langle 110\rangle$, $a_0 = 0.364$ nm, which gives a Burger vector magnitude of 0.257 nm, allows a comparison of the current hardening results with the DBH model predictions.

Higgy and Hammed showed a linear relationship between the yield stress and hardness of the form [94].

$$\Delta H = K\Delta\sigma_y \tag{2}$$

where the constant K is ~3 for irradiated austenitic stainless steels [94,95]. Using Equations (1) and (2), the hardness increment (ΔH_c) based on the DBH model can be calculated.

Table 3 shows the comparison between the calculated hardness changes ΔH_c and the experimentally obtained hardness changes ΔH_e for the irradiated samples. It can be seen that the calculated hardness changes using the DBH model are consistent with hardness changes obtained by nano-indentation tests. A small difference in experimental values and the calculated values for 0.3 dpa irradiation at room temperature could be due to the presence of additional non-visible defects clusters which are not detected by TEM. Overall it appears that the visible dislocation loops are the main contributors for irradiation induced hardening of HEAs at room temperature and higher temperature irradiations.

4. Discussion

The purpose of this study is to obtain initial experimental data on the irradiation behavior of a novel single phase FCC high entropy alloy over a wide range of technology-relevant temperatures. It is generally accepted that radiation enhances the diffusion in solids by creating defects such as vacancies and interstitials. Unlike in conventional alloys, each atom in the HEA is surrounded by different neighboring atoms leading to different bond configurations and thus different lattice potential energies (LPE) at lattice sites. If one atom has to diffuse from one lattice position to another position, it will most likely be in different environment with a different lattice potential energy. The new lattice position may not be energetically preferable for the atom, so in order to minimize its energy the atom may return back to its original position or might find a new location having similar neighboring atoms. This qualitative discussion suggests the atomic diffusion in HEAs may be suppressed due to the anticipated existence of preferential lattice sites for each element which could lead to suppression of diffusion. Tsai et al., has reported the diffusion kinetics of each element in the Co-Cr-Fe-Mn-Ni HEA system are lower than conventional alloys [89]. For example, Cr and Ni diffusion coefficients in Co-Cr-Fe-Mn-Ni HEA were reported to be 2.5 and 2.8 times slower than the diffusion in FCC-Fe [96]. Similarly in the current Fe-Ni-Mn-Cr HEA, sluggish solute diffusion might suppress the radiation-induced segregation behavior, as the different constituent elements have to diffuse in a coordinated manner against the fluctuating potential energies at the lattice sites.

4.1. Severe lattice distortion effect

Since every atom in a multicomponent matrix is surrounded by different kinds of atoms, a lattice strain due to atomic size difference is expected. This lattice strain could produce preferential diffusion of certain solute atoms and therefore we quantify the magnitude of this alternative diffusion mechanism in the following. The difference in atomic radius ΔR, can be calculated using the equation below.

$$\Delta R_{max} = (R_i - R_a)/R_a \tag{3}$$

$$R_a = \sum_{i=1}^{n} R_i C_i \tag{4}$$

where R_a is the average atomic radius, R_i is atomic radius of component and C_i is the molar percent of component. The atomic radius of Fe is 0.124 nm, Ni is 0.125 nm, Mn is 0.112 nm and Cr is 0.125 nm, using estimates based on metallic bonding [97,98].

Based on above equation, the calculated maximum difference in the atomic radius in near-equimolar 27Fe-28Ni-27Mn-18Cr HEA is ΔR_{max} is 7.6%. Since the maximum calculated misfit between the solute atoms is ≈ 7.6%, which is less than the 12% limit for solid solution stability [98], the segregation due to the contribution from elastic strain energy associated with misfit atom lattice distortion is assumed to be minimal in Fe-Ni-Mn-Cr.

Table 3
Comparison of calculated hardness change (ΔH_c) and experimentally obtained hardness change (ΔH_e), in the ion irradiated Fe-Ni-Mn-Cr HEA specimens.

Irradiation temperature (°C)	Dose (dpa)	Experimental change in hardness ΔH_e (GPa)	Calculated change in hardness ΔH_p (GPa)
RT	0.03	0.92	1.06
RT	0.3	2.31	1.59
500	0.3	0.33	0.39
500	3	0.47	0.46

4.2. High entropy effect

The contribution of configurational entropy in reduction of the total Gibbs free energy will be high only when the alloy microstructure is single-phase [96]. Buildup of large local defect concentrations during irradiation can introduce noticeable changes in stability of phases. Otto et al. [99] have shown that entropies can vary substantially in equal element multi-component alloys and other factors such as chemical interactions between the elements play an important role in single phase stability. In addition, it was reported that equiatomic binary pairs: Fe-Ni, Ni-Cr, Fe-Mn, Fe-Cr, Ni-Mn, exhibit small calculated deviations in entropy and Gibbs free energy from ideal fcc solid solutions at high temperatures, suggesting that a single phase solid solution is energetically favorable [99]. In the current Fe-Ni-Mn-Cr HEA alloy, phase decomposition was not observed at any irradiation condition, which is consistent with high configurational entropy playing a crucial role in single phase stability. Nevertheless, the specific physical mechanism responsible for the good phase stability (e.g., high configuration entropy vs. sluggish diffusion that inhibits achievement of equilibrium conditions or other potential mechanisms) requires further investigation. Detailed kinetic calculations are needed to understand the entropy effect on the solute segregation and subsequent precipitation behavior in HEAs. Lack of thermodynamic and kinetic databases on HEAs in the literature restricts a deeper understanding of their segregation behavior. Regardless of the specific physical mechanism, it can be clearly concluded that, compared to conventional austenitic Fe-Cr-Ni and Fe-Cr-Mn alloys, a significant difference in radiation response of the Fe-Ni-Mn-Cr HEA at elevated irradiation temperatures (400–700 °C) is observed.

Comparison of the present experimental results with those observed in conventional Fe-Cr-Ni alloys, such as lower radiation-induced segregation at the grain boundaries, shift in peak radiation induced solute segregation temperature to higher temperatures, lack of visible void formation, and reduced driving force to eliminate defects such as dislocation loops during irradiation in the high temperature regime of 400–700 °C, indicate that the current multi-component Fe-Ni-Mn-Cr alloy could be a promising new type of structural material with high radiation resistance for nuclear energy applications. The apparent sluggish diffusion at 400–700 °C suggests that HEAs may be good candidate materials up to higher operating temperatures compared to conventional austenitic steels.

It is well known that the viability of proposed fusion and advanced fission energy systems are highly dependent on the availability of structural materials that can retain their functionality and integrity under extreme reactor conditions throughout its lifetime. Several materials are currently under consideration, including ferritic-martensitic steels with high void swelling resistance [100–102], compositionally tailored austenitic steels [103], ODS ferritic steel [104–106], SiC/SiC composites [107,108], nano-engineered austenitic stainless steels [109], and V alloys [110,111]. However, nearly all these materials are still at a relatively early stage of development and have their own sets of limitations. For example, ferritic-martensitic steels generally exhibit good unirradiated properties and have good void swelling and RIS resistance at intermediate temperatures, but suffer from relatively poor thermal creep strength at high temperatures (>550 °C) and are susceptible to radiation-induced fracture toughness embrittlement at low temperatures. The required performance parameters for structural materials in the extremely harsh fission and fusion reactor radiation environment are very challenging, so the conventional physical metallurgy approach based on only one dominant solvent may not enable the requisite dramatic improvements in properties. Therefore exploration of new classes of potentially revolutionary materials is valuable. High entropy alloys have shown many promising properties for structural applications such as lesser degree of softening than conventional alloys especially at elevated temperatures [112–115]. However, considerable additional research is needed to confirm the appropriateness of HEAs for nuclear energy applications. The results presented in this study are an encouraging initial investigation of the potential applicability of HEAs for nuclear energy structural applications. Further research on the irradiation damage resistance of high entropy alloys should be conducted, including irradiations to higher doses to confirm and extend the current moderate-dose (~10 dpa) observation of good radiation resistance. Further improvements in structural performance and radiation resistance by purposeful introduction of alloy modifications, such as grain boundary engineering [116] and/or precipitates to serve as efficient point defect recombination sinks [117,118], can be envisioned.

5. Conclusions

In the present experimental study, the irradiation behavior of Fe-28%Ni-27%Mn-18%Cr high entropy alloy specimens irradiated at temperatures ranging from room temperature to 700 °C to mid-range doses of 0.1–10 dpa has been examined. Microstructural changes and associated hardening in the irradiated HEA is qualitatively similar to conventional austenitic Fe-Cr-Ni or Fe-Cr-Mn alloys for irradiation near room temperature. Conversely, microstructural characterization performed using transmission electron microscopy shows that the radiation damage changes at elevated temperatures (400–700 °C) are generally markedly different (less radiation degradation) in the examined FCC Fe-Ni-Mn-Cr high entropy alloy compared to conventional austenitic Fe-Cr-Ni or Fe-Cr-Mn alloys.

- Fe-Ni-Mn-Cr high entropy alloy did not exhibit any phase instability after ion irradiation up to midrange doses of 10 dpa at 400–700 °C.
- The radiation-induced solute segregation (RIS) behavior near grain boundaries in the examined Fe-Ni-Mn-Cr HEA specimens is significantly suppressed compared to the behavior observed in Fe-Cr-Ni and Fe-Cr-Mn austenitic alloys.
- Void formation was not observed at any irradiation condition. Since Fe-Cr-Ni alloys typically experience ~1% volumetric void swelling at comparable ion irradiation conditions, this indicates

that the Fe-Ni-Mn-Cr HEA has better swelling resistance than conventional Fe-Cr-Ni austenitic alloys.
- The lower defect cluster size and higher cluster density for the irradiated Fe-Ni-Mn-Cr HEA compared to conventional Fe-Cr-Ni alloys at 400–700 °C, along with the shift in the peak radiation induced solute segregation regime to higher temperatures, is consistent with reduced point defect mobility for HEAs.

Collectively, these observations suggest that high entropy alloys are promising base compositions for demanding nuclear energy applications, and more generally that high configurational entropy may exert a significant influence on microstructural evolution in irradiated materials at elevated temperatures relevant for advanced nuclear energy applications.

Acknowledgements

The authors gratefully acknowledge Dr. Yanwen Zhang, Dr. Lin Shao and research staff at IBML-UTK and REF-TAMU, for performing the ion irradiations. We thank Dr. Chad Parish for his assistance in operating Talos F200X microscope. This research and operation of the Talos F200X transmission electron microscope was supported by the Office of Fusion Energy Science, US Department of Energy under contract DE-AC05-00OR22725 with UT-Battelle, LLC.

References

[1] M.C. Troparevsky, J.R. Morris, M. Daene, Y. Wang, A.R. Lupini, G.M. Stocks, Beyond atomic sizes and Hume-Rothery rules: understanding and predicting high-entropy alloys, JOM 67 (2015) 2350–2363.
[2] J.W. Yeh, S.K. Chen, S.J. Lin, J.Y. Gan, T.S. Chin, T.T. Shun, C.H. Tsau, S.Y. Chang, Nanostructured high-entropy alloys with multiple principal elements: novel alloy design concepts and outcomes, Adv. Eng. Mater. 6 (2004) 299–303.
[3] J.-W. Yeh, S.-J. Lin, T.-S. Chin, J.-Y. Gan, S.-K. Chen, T.-T. Shun, C.-H. Tsau, S.-Y. Chou, Formation of simple crystal structures in Cu-Co-Ni-Cr-Al-Fe-Ti-V alloys with multiprincipal metallic elements, Metall. Mater. Trans. A 35 (2004) 2533–2536.
[4] Y.J. Zhou, Y. Zhang, Y.L. Wang, G.L. Chen, Solid solution alloys of AlCoCrFeNiTix with excellent room-temperature mechanical properties, Appl. Phys. Lett. 90 (2007) 181904.
[5] C.-Y. Hsu, J.-W. Yeh, S.-K. Chen, T.-T. Shun, Wear resistance and high-temperature compression strength of Fcc CuCoNiCrAl0.5Fe alloy with boron addition, Metall. Mater. Trans. A 35 (2004) 1465–1469.
[6] C.-M. Lin, H.-L. Tsai, Equilibrium phase of high-entropy FeCoNiCrCu0.5 alloy at elevated temperature, J. Alloys Compd. 489 (2010) 30–35.
[7] T. Nagase, P.D. Rack, J.H. Noh, T. Egami, In-situ TEM observation of structural changes in nano-crystalline CoCrCuFeNi multicomponent high-entropy alloy (HEA) under fast electron irradiation by high voltage electron microscopy (HVEM), Intermetallics 59 (2015) 32–42.
[8] S.Q. Xia, X. Yang, T.F. Yang, S. Liu, Y. Zhang, Irradiation resistance in AlxCoCrFeNi high entropy alloy, JOM 67 (2015) 2340–2344.
[9] A. Etienne, B. Radiguet, N.J. Cunningham, G.R. Odette, R. Valiev, P. Pareige, Comparison of radiation-induced segregation in ultrafine-grained and conventional 316 austenitic stainless steels, Ultramicroscopy 111 (2011) 659–663.
[10] T. Nagase, S. Anada, P.D. Rack, J.H. Noh, H. Yasuda, H. Mori, T. Egami, MeV electron-irradiation-induced structural change in the bcc phase of Zr-Hf-Nb alloy with an approximately equiatomic ratio, Intermetallics 38 (2013) 70–79.
[11] E.A. Kenik, J.T. Busby, Radiation-induced degradation of stainless steel light water reactor internals, Mater. Sci. Eng. R Rep. 73 (2012) 67–83.
[12] A.J. Ardell, P. Bellon, Radiation-induced solute segregation in metallic alloys, Curr. Opin. Sol. State Mater. Sci. (2016), http://dx.doi.org/10.1016/j.cossms.2015.11.001 in press, http://www.sciencedirect.com/science/article/pii/S1359028615300097.
[13] M. Nastar, F. Soisson, Radiation-induced segregation, in: R.J.M. Konings (Ed.), Comprehensive Nuclear Materials, vol. 1, Elsevier, Amsterdam, 2012, pp. 471–496.
[14] T. Egami, M. Ojha, O. Khorgolkhuu, D.M. Nicholson, G.M. Stocks, Local electronic effects and irradiation resistance in high entropy alloys, JOM 67 (2015) 2345–2349.
[15] S.Q. Xia, Z. Wang, T.F. Yang, Y. Zhang, Irradiation behavior in high entropy alloys, J. Iron Steel Res. Int. 22 (2015) 879–884.
[16] Y. Zhang, G.M. Stocks, K. Jin, C. Lu, H. Bei, B.C. Sales, L. Wang, L.K. Beland, R.E. Stoller, G.D. Samolyuk, M. Caro, A. Caro, W.J. Weber, Influence of chemical disorder on energy dissipation and defect evolution in concentrated solid solution alloys, Nat. Commun. 6 (2015) 8736.
[17] S.J. Zinkle, G.S. Was, Materials challenges in nuclear energy, Acta Mater. 61 (2013) 735–758.
[18] F.A. Garner, Radiation damage in austenitic steels, in: R.J.M. Konings (Ed.), Comprehensive Nuclear Materials, Elsevier, Oxford, 2012, pp. 33–95.
[19] B. Raj, M. Vijayalakshmi, Ferritic steels and advanced ferritic–martensitic steels, in: R.J.M. Konings (Ed.), Comprehensive Nuclear Materials, Elsevier, Oxford, 2012, pp. 97–121.
[20] H.M. Chung, U.S. Nuclear Regulatory Commission, Office of Nuclear Regulatory Research. Division of Engineering Technology. & Argonne National Laboratory, 2006. Assessment of void swelling in austenitic stainless steel core internals. NUREG/CR-6897.
[21] S.M. Bruemmer, E.P. Simonen, P.M. Scott, P.L. Andresen, G.S. Was, J.L. Nelson, Radiation-induced material changes and susceptibility to intergranular failure of light-water-reactor core internals, J. Nucl. Mater 274 (1999) 299–314.
[22] G.S. Was, J.P. Wharry, B. Frisbie, B.D. Wirth, D. Morgan, J.D. Tucker, T.R. Allen, Assessment of radiation-induced segregation mechanisms in austenitic and ferritic–martensitic alloys, J. Nucl. Mater 411 (2011) 41–50.
[23] S. Dumbill, T.M. Williams, Proc. Conf. Materials for Nuclear Reactor Core Applications, vol. 1, British Nuclear Energy Society, London, 1987, p. 119.
[24] G. Gupta, Z. Jiao, A.N. Ham, J.T. Busby, G.S. Was, Microstructural evolution of proton irradiated T91, J. Nucl. Mater 351 (2006) 162–173.
[25] R.E. Clausing, L. Heatherly, R.G. Faulkner, A.F. Rowcliffe, K. Farrell, Radiation-induced segregation in HT-9 martensitic steel, J. Nucl. Mater. 141–143 (Part 2) (1986) 978–981.
[26] Z. Lu, R.G. Faulkner, N. Sakaguchi, H. Kinoshita, H. Takahashi, P.E.J. Flewitt, Effect of hafnium on radiation-induced inter-granular segregation in ferritic steel, J. Nucl. Mater 351 (2006) 155–161.
[27] S. Ohnuki, H. Takahashi, T. Takeyama, Void swelling and segregation of solute in ion-irradiated ferritic steels, J. Nucl. Mater 104 (1981) 1121–1125.
[28] H. Takahashi, S. Ohnuki, T. Takeyama, H. Kayano, The effect of irradiation and post-irradiation annealing on the yield stress and microstructure of vanadium-carbon alloys, J. Nucl. Mater 96 (1981) 233–242.
[29] H. Takahashi, F.A. Garner, H. Itoh, B. Hu, S. Ohnuki, The behavior of solute segregation and void formation in Fe-Cr-Ni and Fe-Cr-Mn steels during electron irradiation, in: F.A. Garner, N.H. Packan, A.S. Kumar (Eds.), Radiation-induced Changes in Microstructure: 13th International Symposium (Part I), American Society and Materials, Philadelphia, 1987, p. 268. ASTM STP 955.
[30] D.S. Bae, S.P. Lee, Y.R. Cho, H. Takahashi, Effect of aging treatment on irradiation-induced segregation of high Mn-Cr steel, Trans. Nonferrous Metals Soc. China 21 (Suppl. 1) (2011) s58–s61.
[31] S. Choudhury, L. Barnard, J.D. Tucker, T.R. Allen, B.D. Wirth, M. Asta, D. Morgan, Ab-initio based modeling of diffusion in dilute bcc Fe–Ni and Fe–Cr alloys and implications for radiation induced segregation, J. Nucl. Mater 411 (2011) 1–14.
[32] T.P.C. Klaver, D.J. Hepburn, G.J. Ackland, Defect and solute properties in dilute Fe-Cr-Ni austenitic alloys from first principles, Phys. Rev. B 85 (2012) 174111.
[33] G. Bonny, N. Castin, D. Terentyev, Interatomic potential for studying ageing under irradiation in stainless steels: the FeNiCr model alloy, Model. Simul. Mater. Sci. Eng. 21 (2013) 085004.
[34] L. Barnard, J.D. Tucker, S. Choudhury, T.R. Allen, D. Morgan, Modeling radiation induced segregation in Ni–Cr model alloys from first principles, J. Nucl. Mater 425 (2012) 8–15.
[35] V.A. Pechenkin, V.L. Molodtsov, V.A. Ryabov, D. Terentyev, On the radiation-induced segregation: contribution of interstitial mechanism in Fe–Cr alloys, J. Nucl. Mater 433 (2013) 372–377.
[36] Z. Wu, H. Bei, Microstructures and mechanical properties of compositionally complex Co-free FeNiMnCr18 FCC solid solution alloy, Mater. Sci. Eng. A 640 (2015) 217–224.
[37] James F. Ziegler, SRIM software. Retrieved July 2015, from http://www.srim.org/.
[38] R.E. Stoller, M.B. Toloczko, G.S. Was, A.G. Certain, S. Dwaraknath, F.A. Garner, On the use of SRIM for computing radiation damage exposure, Nucl. Instrum. Methods Phys. Res. Sect. B Beam Interact. Mater. Atoms 310 (2013) 75–80.
[39] D.L. Plumton, W.G. Wolfer, Suppression of void nucleation by injected interstitials during heavy ion bombardment, J. Nucl. Mater 120 (1984) 245–253.
[40] F.A. Garner, Impact of the injected interstitial on the correlation of charged particle and neutron-induced radiation damage, J. Nucl. Mater 117 (1983) 177–197.
[41] G.S. Was, R.S. Averback, Radiation damage using ion beams, in: R.J.M. Konings (Ed.), Comprehensive Nuclear Materials, vol. 1, Elsevier, Amsterdam, 2012, pp. 195–221.
[42] W.C. Oliver, G.M. Pharr, An improved technique for determining hardness and elastic modulus using load and displacement sensing indentation experiments, J. Mater. Res. 7 (1992) 1564–1583.
[43] W.D. Nix, H. Gao, Indentation size effects in crystalline materials: a law for strain gradient plasticity, J. Mech. Phys. Solids 46 (1998) 411–425.
[44] S.J. Zinkle, Y. Matsukawa, Observation and analysis of defect cluster production and interactions with dislocations, J. Nucl. Mater. 329–333 (Part A) (2004) 88–96.
[45] J. Gan, E.P. Simonen, S.M. Bruemmer, L. Fournier, B.H. Sencer, G.S. Was, The effect of oversized solute additions on the microstructure of 316SS irradiated

with 5 MeV Ni++ ions or 3.2 MeV protons, J. Nucl. Mater 325 (2004) 94–106.
[46] T. Okita, T. Sato, N. Sekimura, T. Iwai, F.A. Garner, The synergistic influence of temperature and displacement rate on microstructural evolution of ion-irradiated Fe–15Cr–16Ni model austenitic alloy, J. Nucl. Mater. 367–370 (Part B) (2007) 930–934.
[47] A. Etienne, M. Hernández-Mayoral, C. Genevois, B. Radiguet, P. Pareige, Dislocation loop evolution under ion irradiation in austenitic stainless steels, J. Nucl. Mater 400 (2010) 56–63.
[48] T. Muroga, F.A. Garner, J.M. McCarthy, N. Yoshida, The influence of nickel content on microstructures of Fe-Cr-Ni austenitic ternaries irradiated with fast neutrons or heavy ions, in: Radiation Effects on Materials: 15th International Symposium, ASTM STP 1125, American Soc. for Testing and Materials, West Conshohocken, PA, 1992, p. 1015.
[49] S.G. McDonald, A. Taylor, Void swelling behavior of types 304 and 316 Stainless steel irradiated with 4-MeV Ni^+ ions, in: Effects of Radiation Effects on Substructures and Mechanical Properties of Metals and Alloys, ASTM STP 529, American Soc. for Testing and Materials, West Conshohocken, PA, 1973, p. 228.
[50] H.-H. Jin, E. Ko, S. Lim, J. Kwon, Effects of helium and hydrogen on radiation-induced microstructural changes in austenitic stainless steel, Nucl. Instrum. Methods Phys. Res. Sect. B Beam Interact. Mater. Atoms 359 (2015) 69–74.
[51] K. Shiraishi, K. Fukai, E. Yagi, Damage profiles in a stainless steel irradiated with Ar and N ions, J. Nucl. Mater. 179–181 (Part 1) (1991) 550–553.
[52] S. Wood, J.A. Spitznagel, W.J. Choyke, N.J. Doyle, J.N. McGruer, J.R. Townsend, Microstructural development in dual ion bombarded 316 stainless steel, in: Effects of Radiation on Materials: 10th International Symposium, ASTM STP 725, Amer. Soc. for Testing and Materials, West Conshohocken, PA, 1980, p. 455.
[53] Q. Xu, H. Watanabe, N. Yoshida, Microstructural evolution in FeCrNi alloy irradiated with Ni ion under varying temperature, J. Nucl. Mater. 233–237 (Part 2) (1996) 1057–1061.
[54] E.H. Lee, T.S. Byun, J.D. Hunn, M.H. Yoo, K. Farrell, L.K. Mansur, On the origin of deformation microstructures in austenitic stainless steel: part I—microstructures, Acta Mater. 49 (2001) 3269–3276.
[55] H.F. Huang, J.J. Li, D.H. Li, R.D. Liu, G.H. Lei, Q. Huang, L. Yan, TEM, XRD and nanoindentation characterization of xenon ion irradiation damage in austenitic stainless steels, J. Nucl. Mater 454 (2014) 168–172.
[56] T.M. Williams, The effect of soluble carbon on void swelling and low dose dislocation structures in type 316 austenitic stainless steel irradiated with 46.5 MeV Ni6+ ions, J. Nucl. Mater 88 (1980) 217–225.
[57] J.A. Hudson, Void formation in solution-treated AISI 316 and 321 stainless-steels under 46.5 MeV NI6+ irradiation, J. Nucl. Mater 60 (1976) 89–106.
[58] T.M. Williams, Interstitial loop nucleation and growth in solution-treated type-316 stainless-steel irradiated to low-doses with 22 MeV C2+ and 46.5 MeV NI6+ ions, J. Nucl. Mater 79 (1979) 28–42.
[59] P.J. Maziasz, Temperature dependence of the dislocation microstructure of PCA austenitic stainless steel irradiated in ORR spectrally-tailored experiments, J. Nucl. Mater. 191–194 (Part B) (1992) 701–705.
[60] P.J. Maziasz, *Trans. Am.* Nucl. Soc. 39 (1981) 433–485.
[61] B.N. Singh, S.J. Zinkle, Defect accumulation in pure fcc metals in the transient regime: a review, J. Nucl. Mater 206 (1993) 212–229.
[62] S.J. Zinkle, P.J. Maziasz, R.E. Stoller, Dose dependence of the microstructural evolution in neutron-irradiated austenitic stainless steel, J. Nucl. Mater 206 (1993) 266–286.
[63] J.F. Stubbins, Void swelling and radiation-induced phase transformation in high purity Fe-Ni-Cr alloys, J. Nucl. Mater. 141–143 (Part 2) (1986) 748–753.
[64] M. Lambrecht, L. Malerba, Positron annihilation spectroscopy on binary Fe–Cr alloys and ferritic/martensitic steels after neutron irradiation, Acta Mater. 59 (2011) 6547–6555.
[65] H.K.D.H. Bhadeshia, Recrystallisation of practical mechanically alloyed iron-base and nickel-base superalloys, Mater. Sci. Eng. A 223 (1997) 64–77.
[66] F.A. Garner, M.B. Toloczko, B.H. Sencer, Comparison of swelling and irradiation creep behavior of fcc-austenitic and bcc-ferritic/martensitic alloys at high neutron exposure, J. Nucl. Mater 276 (2000) 123–142.
[67] E.A. Little, D.A. Stow, Void-swelling in irons and ferritic steels: II. An experimental survey of materials irradiated in a fast reactor, J. Nucl. Mater 87 (1979) 25–39.
[68] S. Ohnuki, F.A. Garner, H. Takahashi, Phase instability and void formation in neutron-irradiated Fe-Cr-Mn-Ni alloys, Mater. Trans. JIM 34 (1993) 1031–1035.
[69] N.H. Packan, K. Farrell, Radiation-induced swelling in an austenitic alloy - observations and interpretation of the effects of helium, Nucl. Technol. Fusion 3 (1983) 392–404.
[70] F.A. Garner, J.M. McCarthy, in: R.L. Klueh, D.S. Gelles, M.Okada, N.H. Packan (Eds.), An Assessment of Fe-Cr-Mn Austenitic Alloys for Fusion Service Using Fast Reactor Irradiation, Reduced Activation Materials for Fusion Reactors, ASTM STP 1047, American Society for Testing and Materials, Philadelphia, 1990, p. 19.
[71] F.A. Garner, H.R. Brager, D.S. Gelles, J.M. McCarthy, Neutron irradiation of Fe-Mn, Fe-Cr-Mn and Fe-Cr-Ni alloys and an explanation of their differences in swelling behavior, J. Nucl. Mater 148 (1987) 294–301.
[72] S. Watanabe, Y. Takamatsu, N. Sakaguchi, H. Takahashi, Sink effect of grain boundary on radiation-induced segregation in austenitic stainless steel, J. Nucl. Mater. 283–287 (Part 1) (2000) 152–156.
[73] G.S. Rohrer, Measuring and interpreting the structure of grain-boundary networks, J. Am. Ceram. Soc. 94 (2011) 633–646.
[74] A.D. Marwick, Segregation in irradiated alloys: the inverse Kirkendall effect and the effect of constitution on void swelling, J. Phys. F. Met. Phys. 8 (1978) 1849.
[75] A.D. Marwick, R.C. Piller, M.E. Horton, Radiation-induced Segregation in Fe-Cr-Ni Alloys. Dimensional Stability and Mechanical Behaviour of Irradiated Metals and Alloys, British Nuclear Energy Society, London, 1984, p. 11.
[76] J.M. Perks, A.D. Marwick, C.A. English, A computer code to calculate radiation-induced segregation in concentrated ternary alloys, United Kingdom (1986) p.42.
[77] H. Wiedersich, P.R. Okamoto, N.Q. Lam, A theory of radiation-induced segregation in concentrated alloys, J. Nucl. Mater 83 (1979) 98–108.
[78] N.Q. Lam, A. Kumar, H. Wiedersich, Kinetics of radiation induced segregation in ternary alloys, in: Effects of Radiation on Materials: 11th International Symposium, ASTM STP 782, Amer. Soc. for Testing and Materials, West Conshohocken, PA, 1982, p. 985.
[79] T.R. Allen, J.T. Busby, G.S. Was, E.A. Kenik, On the mechanism of radiation-induced segregation in austenitic Fe–Cr–Ni alloys, J. Nucl. Mater 255 (1998) 44–58.
[80] T.R. Allen, J.T. Busby, J. Gan, E. Kenik, G.S. Was, The correlation between swelling and radiation induced segregation in Fe-Cr-Ni alloys, in: Effects of Radiation on Materials: 19th International Symposium, ASTM STP 1366, Amer. Soc. for Testing and Materials, West Conshohocken, PA, 2000, p. 739.
[81] N. Shigenaka, S. Ono, Y. Isobe, T. Hashimoto, H. Fujimori, S. Uchida, Radiation induced segregation at grain boundary in an austenitic stainless steel under ion irradiation, J. Nucl. Sci. Technol. 33 (1996) 474–478.
[82] E.A. Kenik, Elemental inhomogeneities developed in stainless steels by radiation-induced segregation, J. Nucl. Mater 205 (1993) 317–323.
[83] S.M. Bruemmer, M.D. Merz, L.A. Charlot, A method for evaluating radiation-induced grain-boundary segregation using ion-irradiated microcrystalline stainless alloys, J. Nucl. Mater 186 (1991) 13–19.
[84] G.S. Was, Fundamentals of Radiation Materials Science Metals and Alloys, Springer, Berlin, 2007.
[85] T. Takeyama, H. Takahashi, S. Ohnuki, Radiation induced segregation in austenitic and ferritic steels, Bull. Fac. Eng. Hokkaido Univ. 121 (1984) 85–99.
[86] T.R. Allen, G.S. Was, E.A. Kenik, The effect of alloy composition on radiation-induced segregation in Fe-Cr-Ni alloys, J. Nucl. Mater 244 (1997) 278–294.
[87] D.L. Damcott, T.R. Allen, G.S. Was, Dependence of radiation-induced segregation on dose, temperature and alloy composition in austenitic alloys, J. Nucl. Mater 225 (1995) 97–107.
[88] H. Takahashi, K. Shiba, S. Nakahigashi, S. Ohnuki, H. Kinoshita, F.A. Garner, The effect of composition and phase on segregation of Fe-Cr based alloys, in: Reduced Activation Materials for Fusion Reactors, ASTM STP 1047, Amer. Soc. for Testing and Materials, West Conshohocken, PA, 1990, p. 93.
[89] K.Y. Tsai, M.H. Tsai, J.W. Yeh, Sluggish diffusion in Co–Cr–Fe–Mn–Ni high-entropy alloys, Acta Mater. 61 (2013) 4887–4897.
[90] E. Orowan, Internal Stresses in Metals and Alloys, Institute of Metals, London, 1948, p. 451.
[91] A. Seeger, Proceedings of the 2nd International Conference on Peaceful Uses of Atomic Energy, Geneva, vol. 6, International Atomic Energy Agency, Vienna, Austria, 1958, p. 250.
[92] G.E. Lucas, The evolution of mechanical property changes in irradiated austenitic stainless steel, J. Nucl. Mater 206 (1993) 287–305.
[93] T.S. Byun, N. Hashimoto, K. Farrell, E.H. Lee, Characteristics of microscopic strain localization in irradiated 316 stainless steels and pure vanadium, J. Nucl. Mater 349 (2006) 251–264.
[94] H.R. Higgy, F.H. Hammad, Effect of fast-neutron irradiation on mechanical properties of stainless steels: AISI types 304, 316 and 347, J. Nucl. Mater 55 (1975) 177–186.
[95] J.T. Busby, M.C. Hash, G.S. Was, The relationship between hardness and yield stress in irradiated austenitic and ferritic steels, J. Nucl. Mater 336 (2005) 267–278.
[96] B.S. Murty, J.W. Yeh, S. Ranganathan, High-entropy Alloys, Butterworth-Heinemann, 2014. ISBN : 978-0-12-800251-3.
[97] T. Akira, I. Akihisa, Classification of bulk metallic glasses by atomic size difference, heat of mixing and period of constituent elements and its application to characterization of the main alloying element, Mater. Trans. 46 (2005) 2817–2829.
[98] A. Li, X. Zhang, Thermodynamic analysis of the simple microstructure of AlCrFeNiCu high-entropy alloy with multi-principal elements, Acta Metall. Sin. Engl. Lett. 22 (2009) 219–224.
[99] F. Otto, Y. Yang, H. Bei, E.P. George, Relative effects of enthalpy and entropy on the phase stability of equiatomic high-entropy alloys, Acta Mater. 61 (2013) 2628–2638.
[100] R.L. Klueh, D.S. Gelles, S. Jitsukawa, A. Kimura, G.R. Odette, B. van der Schaaf, M. Victoria, Ferritic/martensitic steels – overview of recent results, J. Nucl. Mater. 307–311 (Part 1) (2002) 455–465.
[101] A.A.F. Tavassoli, A. Alamo, L. Bedel, L. Forest, J.M. Gentzbittel, J.W. Rensman, E. Diegele, R. Lindau, M. Schirra, R. Schmitt, H.C. Schneider, C. Petersen, A.M. Lancha, P. Fernandez, G. Filacchioni, M.F. Maday, K. Mergia, N. Boukos, Baluc, P. Spätig, E. Alves, E. Lucon, Materials design data for reduced activation martensitic steel type EUROFER, J. Nucl. Mater. 329–333 (Part A) (2004) 257–262.
[102] R.L. Klueh, A.T. Nelson, Ferritic/martensitic steels for next-generation

reactors, J. Nucl. Mater 371 (2007) 37–52.
[103] S.J. Zinkle, N.M. Ghoniem, Operating temperature windows for fusion reactor structural materials, Fusion Eng. Des. 51–52 (2000) 55–71.
[104] S. Ukai, M. Fujiwara, Perspective of ODS alloys application in nuclear environments, J. Nucl. Mater. 307–311 (Part 1) (2002) 749–757.
[105] R.L. Klueh, J.P. Shingledecker, R.W. Swindeman, D.T. Hoelzer, Oxide dispersion-strengthened steels: a comparison of some commercial and experimental alloys, J. Nucl. Mater 341 (2005) 103–114.
[106] S.J. Zinkle, Advanced materials for fusion technology, Fusion Eng. Des. 74 (2005) 31–40.
[107] W.E. Windes, P.A. Lessing, Y. Katoh, L.L. Snead, E. Lara-Curzio, J. Klett, C. Henager, R.J. Shinavski, Structural Ceramic Composites for Nuclear Applications, August 2005. INL/EXT-05–00652.
[108] L.L. Snead, T. Nozawa, M. Ferraris, Y. Katoh, R. Shinavski, M. Sawan, Silicon carbide composites as fusion power reactor structural materials, J. Nucl. Mater 417 (2011) 330–339.
[109] C. Sun, S. Zheng, C.C. Wei, Y. Wu, L. Shao, Y. Yang, K.T. Hartwig, S.A. Maloy, S.J. Zinkle, T.R. Allen, H. Wang, X. Zhang, Superior radiation-resistant nanoengineered austenitic 304L stainless steel for applications in extreme radiation environments, Sci. Rep. 5 (2015) 7801.
[110] S.J. Zinkle, H. Matsui, D.L. Smith, A.F. Rowcliffe, E. van Osch, K. Abe, V.A. Kazakov, Research and development on vanadium alloys for fusion applications, J. Nucl. Mater. 258–263 (Part 1) (1998) 205–214.
[111] T. Muroga, J.M. Chen, V.M. Chernov, R.J. Kurtz, M. Le Flem, Present status of vanadium alloys for fusion applications, J. Nucl. Mater 455 (2014) 263–268.
[112] C.-Y. Hsu, C.-C. Juan, W.-R. Wang, T.-S. Sheu, J.-W. Yeh, S.-K. Chen, On the superior hot hardness and softening resistance of AlCoCrxFeMo0.5Ni high-entropy alloys, Mater. Sci. Eng. A 528 (2011) 3581–3588.
[113] W.-R. Wang, W.-L. Wang, J.-W. Yeh, Phases, microstructure and mechanical properties of AlxCoCrFeNi high-entropy alloys at elevated temperatures, J. Alloys Compd. 589 (2014) 143–152.
[114] C.-W. Tsai, Y.-L. Chen, M.-H. Tsai, J.-W. Yeh, T.-T. Shun, S.-K. Chen, Deformation and annealing behaviors of high-entropy alloy Al0.5CoCrCuFeNi, J. Alloys Compd. 486 (2009) 427–435.
[115] W.-H. Wu, C.-C. Yang, L. Yeh, Industrial development of high entropy alloys, Eur. J. Control 31 (2006) 737–747.
[116] K. Lu, L. Lu, S. Suresh, Strengthening materials by engineering coherent internal boundaries at the nanoscale, Science 324 (2009) 349–352.
[117] G.R. Odette, M.J. Alinger, B.D. Wirth, Recent developments in irradiation-resistant steels, Annu. Rev. Mater. Res. 38 (2008) 471–503.
[118] S.J. Zinkle, L.L. Snead, Designing radiation resistance in materials for fusion energy, Annu. Rev. Mater. Res. 44 (2014) 241–267.